Supporting Information

High-entropy solvent design enabling universal electrolyte with a low freezing point for low-temperature aqueous batteries

Huimin Ji,[#a] Chunlin Xie,[#a] Tingqing Wu,[a] Hao Wang,[a] Zhiwen Cai,[a] Qi Zhang,[a] Wenbin Li,[a] Liang Fu,[b,*], Huanhuan Li,[c] and Haiyan Wang[a,*]

a. Hunan Provincial Key Laboratory of Chemical Power Sources, College of Chemistry and Chemical Engineering, Central South University, Changsha, 410083, P.R. China

E-mail: wanghy419@csu.edu.cn

b. College of Materials Science and Engineering, Chongqing University, Chongqing, 400045, P. R. China.

E-mail: liangfu@cqu.edu.cn

c. School of Chemistry and Chemical Engineering, Henan Normal University, Xinxiang 453007, P. R. China.

# These authors contributed equally to this work.

Experimental section

Materials

The zinc foil (30 μm, 99.99%) was purchased from WanKeDa Metallic Materials. Ammonium persulfate ($(NH_4)_2S_2O_8$, AR) and aniline (C_6H_7N, AR) were purchased from Aladdin. Hydrochloric acid (HCl, 36.5 wt%) and zinc sulfate ($ZnSO_4 \cdot 7H_2O$, AR) were purchased from Sinopharm Group Co. Ltd.

Characterizations

A thermal imaging camera (Hangzhou Hikmicro Sensing Technology Co., Ltd.) was used to record the endothermic phenomenon during the dissolution of acetamide. Differential scanning calorimeter (DSC) curves for various solutions were determined by Netzsch DSC 200 F3 with a cooling rate of 6 °C min^{-1} from room temperature to −120 °C under N_2 atmosphere. ^1H and ^{13}C NMR spectra were obtained by a Bruker-600M Hz NMR. The X-ray diffraction (XRD) patterns were recorded at 10-80° using a PANalytical/Empyrean 2 X-ray diffractometer. The morphologies of zinc anodes were characterized by scanning electron microscope (SEM, JEOL/JSM-7610FPlus). Optical microscopy (Nikon Ti2-A) equipped with an in-situ reaction device was used to observe the evolution of zinc deposition. The viscosity of electrolytes at different temperatures was tested by the rheometer (Thermo HAAKE MARS 60) with a heating rate of 5 °C min^{-1} (from −20 °C to 30 °C) under a constant shear rate of 100 s^{-1}.

Preparation of cathodes

Commercial $(NH_4)_2S_2O_8$ (0.183 g) and C_6H_7N (0.298 g) were dissolved in 10 ml HCl (1 M) solution, respectively. The above two solutions were mixed and kept stirring

for 24 h. Then, the obtained precipitate was filtered and washed with deionized water several times. Finally, the polyaniline (PANI) was collected after being dried in a vacuum oven at 80 ºC for 12 h.[1] The PANI and $LiMn_2O_4$ (LMO) cathodes were fabricated by mixing the PANI or LMO, super-P acetylene black, and PVDF with a weight ratio 7:2:1 in NMP solvent. The resulting slurry was coated on stainless steel mesh and dried at 80 °C for 12 h. The active material loading was about 2.2 mg cm^{-2}.

Electrochemical measurements

All cells were assembled with CR2025 coin-type cells with glass fiber as the separator. For symmetric cells and Zn‖PANI full cells, the aqueous 1 M $ZnSO_4$ solution with different amounts of acetamide or formamide was taken as the electrolyte. For Zn‖LMO full cells, 0.5 M $ZnSO_4$ + 0.5 M Li_2SO_4 was taken as the normal electrolyte. The galvanostatic charge-discharge test was carried out using the Neware battery test system at a constant temperature of 30 ºC. Low-temperature battery tests were conducted through an ultra-low-temperature freezer (Heerxin). The Tafel curve was measured by scanning between −0.2 and 0.2 V vs. the open circuit potential at 1mV s^{-1} using Zn‖Zn symmetric cells. The electrochemical stability window of different aqueous electrolytes was measured by linear sweep voltammetry (LSV) at 1 mV s^{-1} in stainless steel foil-stainless steel foil symmetric cells. The ionic conductivity is tested by fabricated symmetric cell, which includes filled electrolyte, and two pieces of stainless-steel foil, and is calculated by the impedance of the electrolyte through the equation as follows:

$$\sigma = \frac{L}{RS} \tag{S1}$$

where σ is ionic conductivity, L is the thickness of the electrolyte (1.15 cm), R is the resistance of the electrolyte, and S is the area of the electrolyte (1.13 cm^{-2}), respectively.

Computational details

The binding energy (E_b) between the molecules was conducted using B3LYP

correlation functional in the DMol3 module of Materials Studio (version 8.0) of

Accelrys Inc according to the following equations:

$$E_b = E_{total} - \sum E_{molecular} \qquad (S2)$$

E_{total} and $E_{molecular}$ represent the total energy energy after binding between molecules

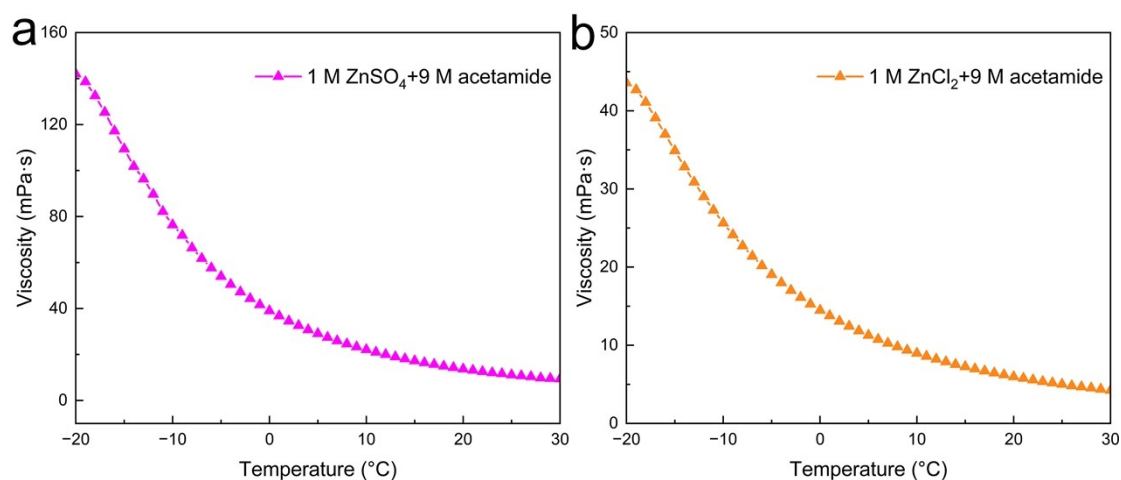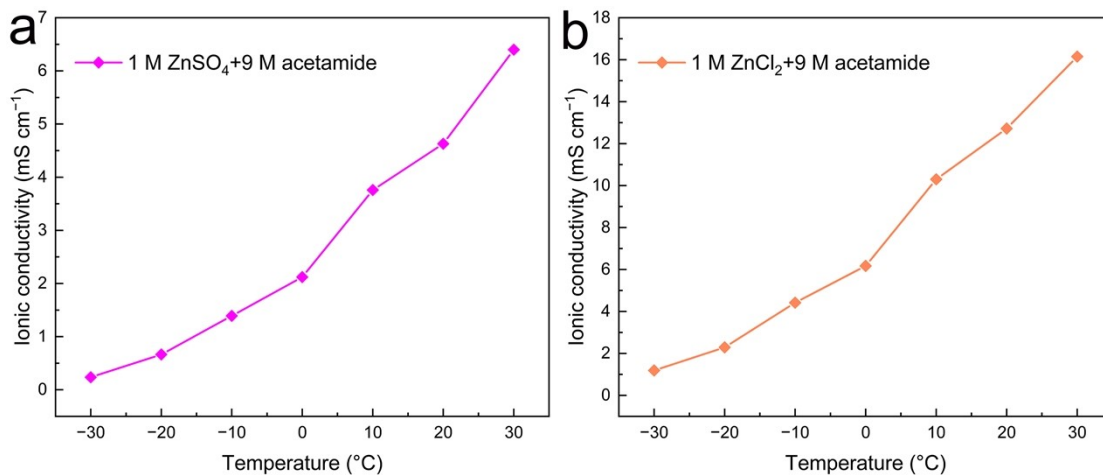and the energy of molecules before binding, respectively.

Fig. S1 Viscosity of 9 M acetamide electrolytes containing (a) 1 M $ZnSO_4$ and (b) 1 M $ZnCl_2$ at different temperatures.

The viscosity of acetamide electrolytes increases upon the decreasing of the temperature. At a low temperature of −20 °C, the acetamide electrolytes still possess relatively low viscosities of 142 mPa s and 44 mPa s for electrolytes containing 1 M $ZnSO_4$ and 1 M $ZnCl_2$ as the salts, respectively. Such low viscosities benefit fast ion transport.

Fig. S2 Ionic conductivity of 9 M acetamide electrolytes containing (a) 1 M $ZnSO_4$ and (b) 1 M $ZnCl_2$ at different temperatures.

The ionic conductivity of acetamide electrolytes decreases upon the decrease of the temperature. At a low temperature of −30 °C, the acetamide electrolytes still possess considerable ionic conductivity of 0.237 mS cm^{-1} and 1.19 mS cm^{-1} for electrolytes containing 1 M $ZnSO_4$ and 1 M $ZnCl_2$ as the salts, respectively. The considerable ionic conductivity allows batteries work well at low temperatures.
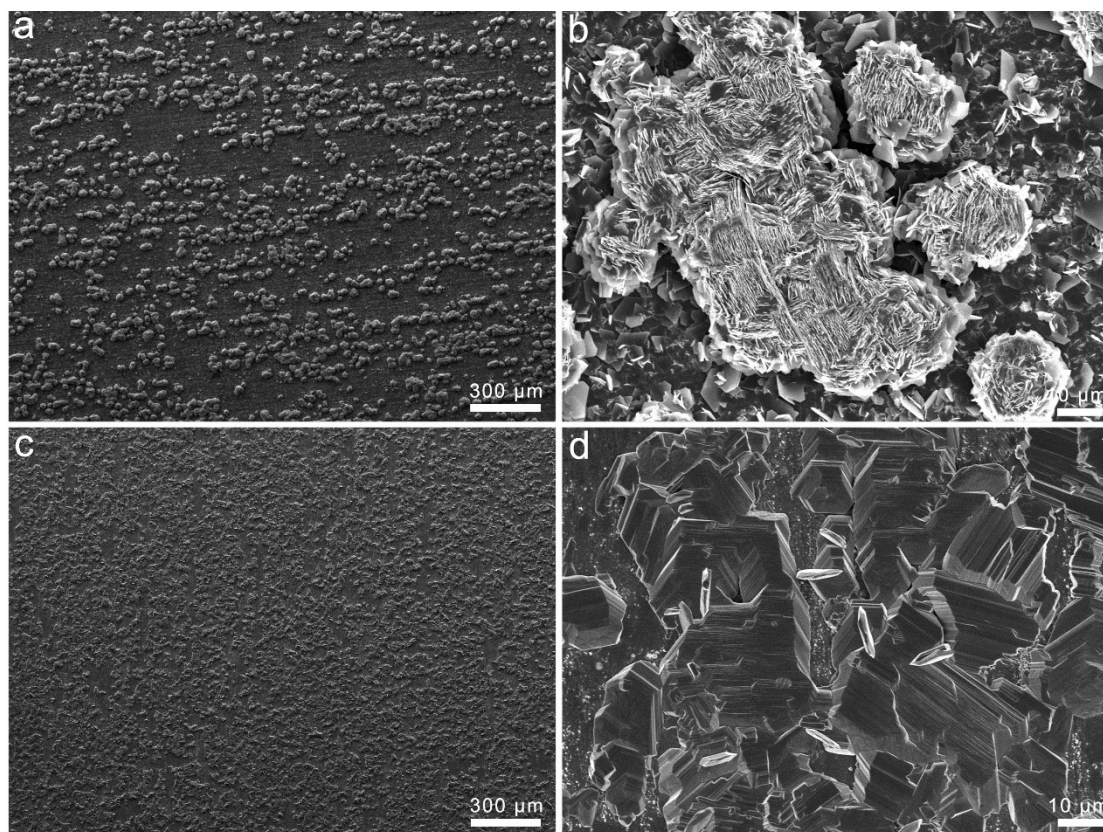
Fig. S3 SEM images of zinc anodes after deposition at 5 mA cm^{-2} for 1 mAh cm^{-2} in

(a, b) 1 M ZnSO$_4$ electrolyte and (c, d) 1 M ZnSO$_4$ + 9 M acetamide electrolyte.
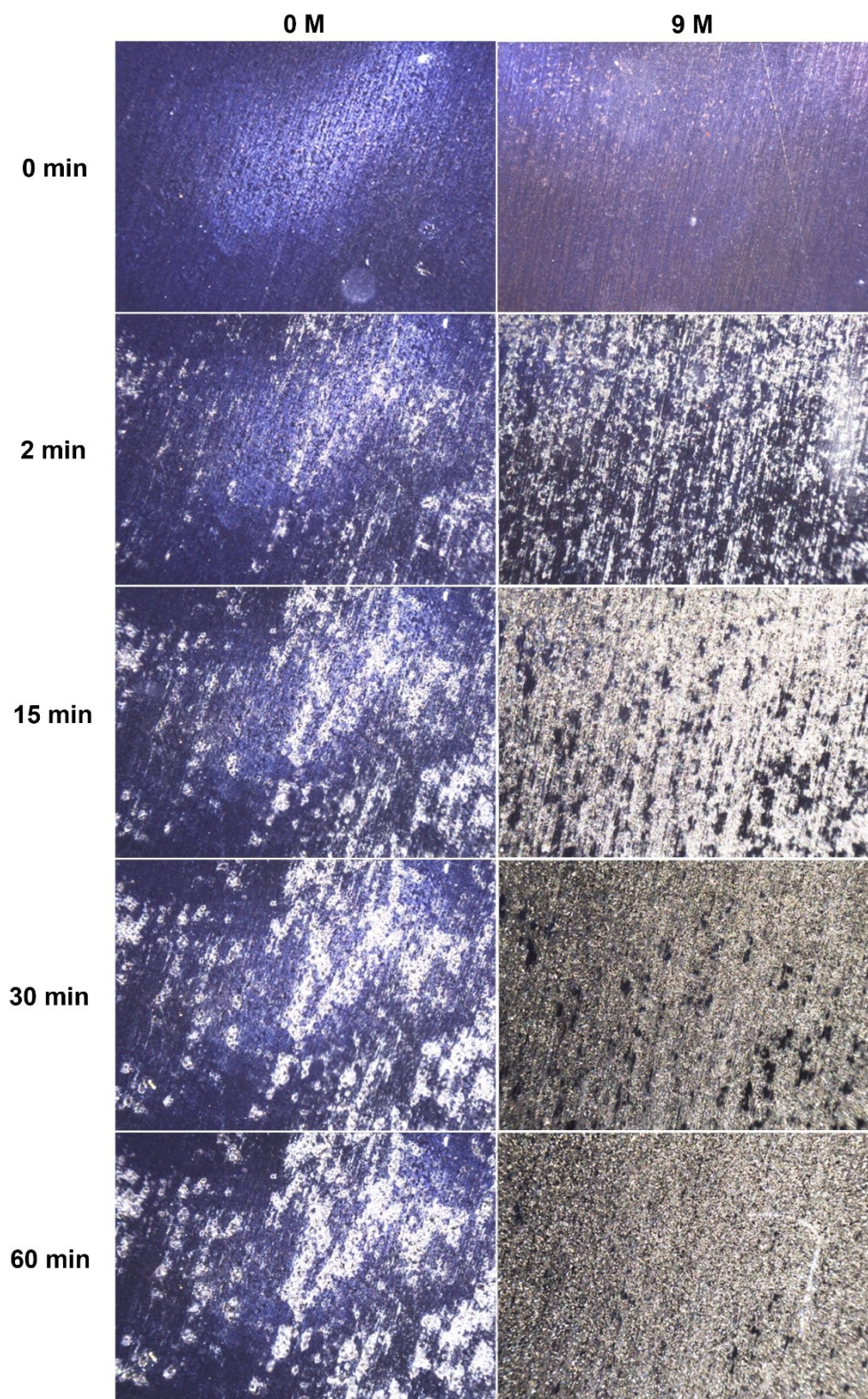
Fig. S4 Top-view in-situ optical microscope observations of zinc deposition using electrolytes with/without acetamide at 5 mA cm^{-2}.
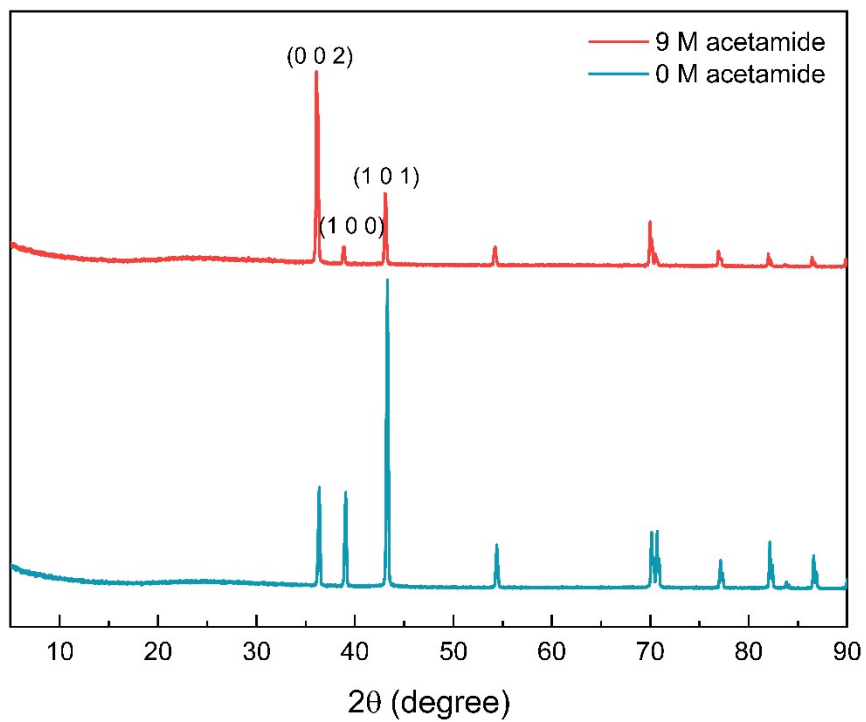
Fig. S5 XRD patterns of zinc anodes after deposition at 5 mA cm^{-2} for 5 mAh cm^{-2} in electrolytes with/without acetamide.
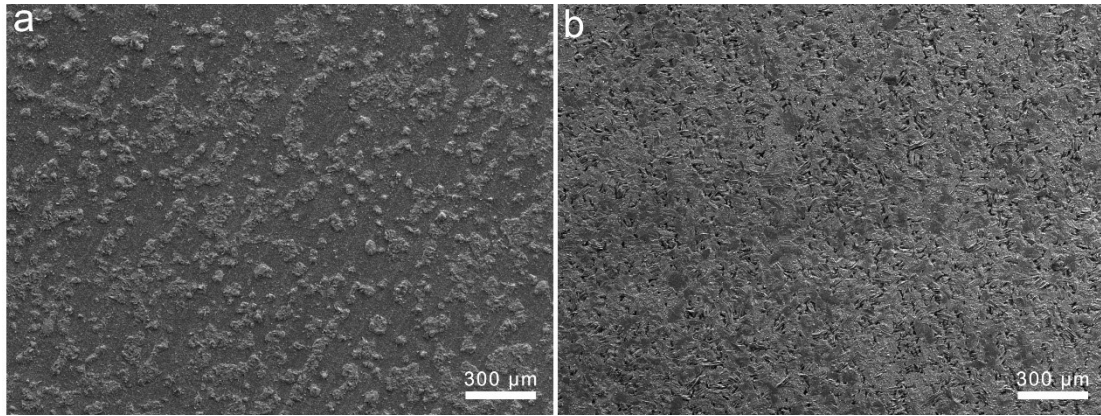
Fig. S6 SEM images of zinc anodes after 40 cycles at 5 mA cm^{-2} for 1 mAh cm^{-2} using electrolytes (a) without or (b) with acetamide.
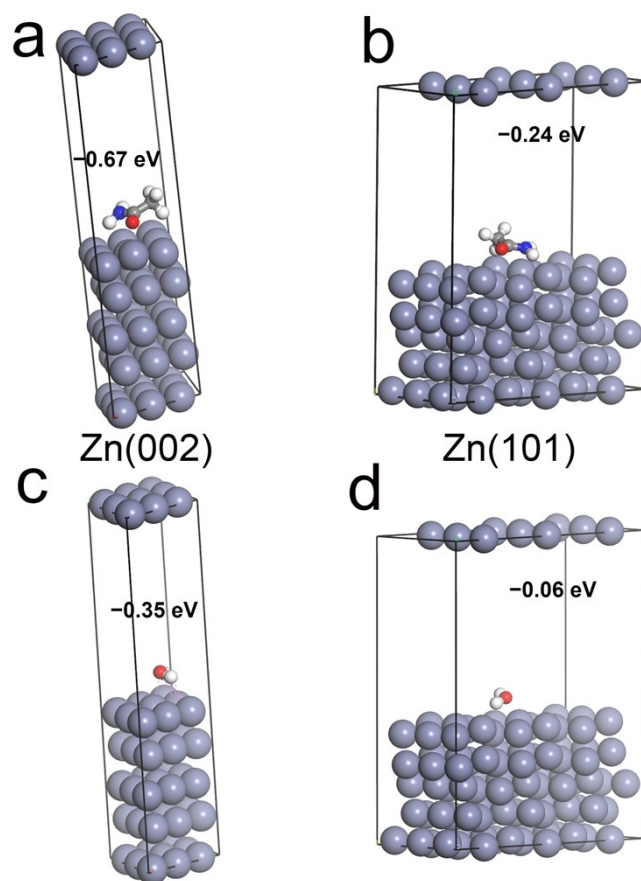
Fig. S7 The binding energy of acetamide and H_2O with Zn(0 0 2) and Zn(1 0 1) facet.

DFT calculations show that acetamide exhibits a higher binding energy than H_2O, indicating the priority of acetamide adsorption on the zinc surface.[2, 3] The preferential adsorption of acetamide instead of water molecules at the zinc facets can alter the composition of electrical double layer structure, suppress interfacial Zn^{2+} ions transfer kinetics, restrict Zn^{2+} ions rampant in-plane diffusion, and homogenize ions flux during zinc deposition, thereby promoting small and dense nuclei rather than large zinc dendrites.[4-6] Moreover, suppressed HER and zinc anode corrosion are also beneficial to suppress zinc dendrite growth.[2, 7, 8]
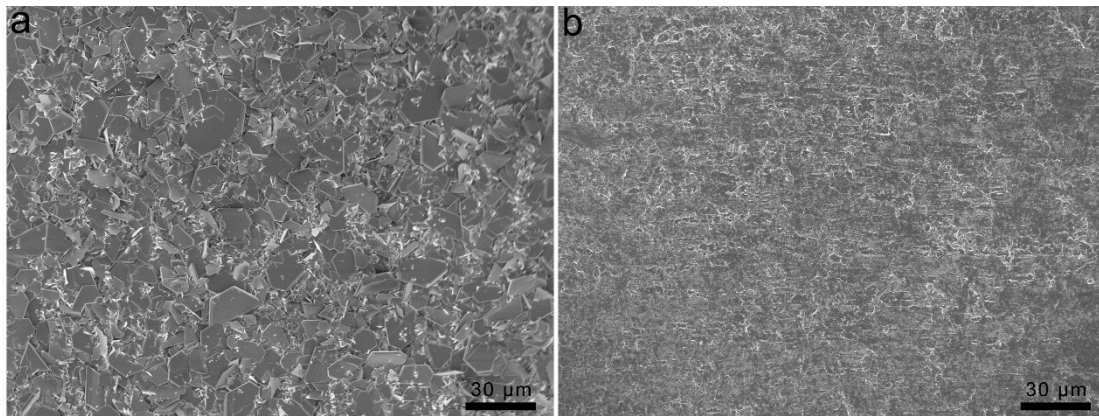
Fig. S8 SEM images of zinc foil after 7 days immersion in (a) 1 M $ZnSO_4$ or (b) 1 M $ZnSO_4$ + 9 M acetamide electrolyte.
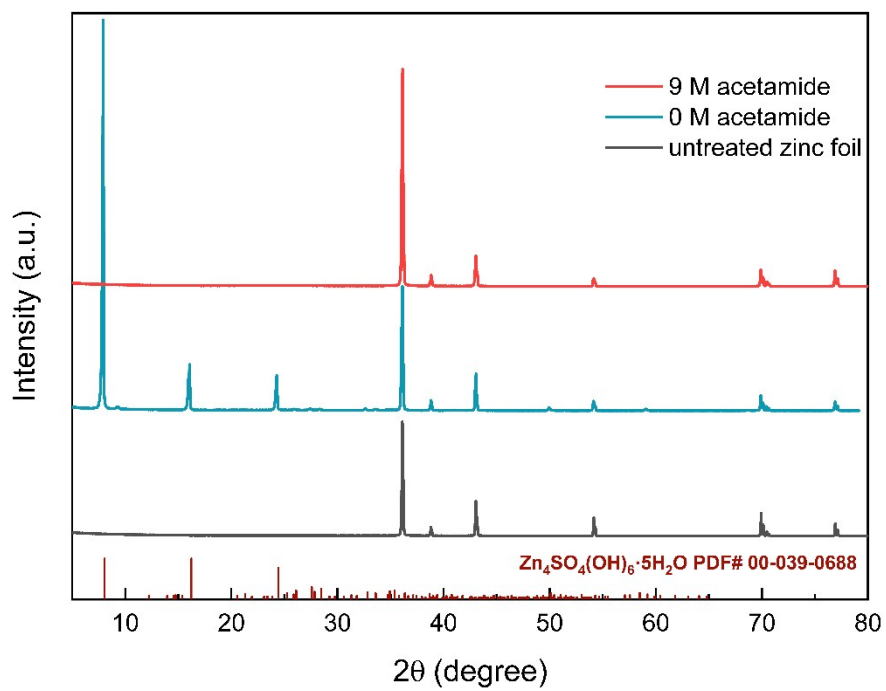
Fig. S9 XRD patterns of zinc foil after 7 days immersion in electrolytes with/without acetamide and untreated zinc foil.
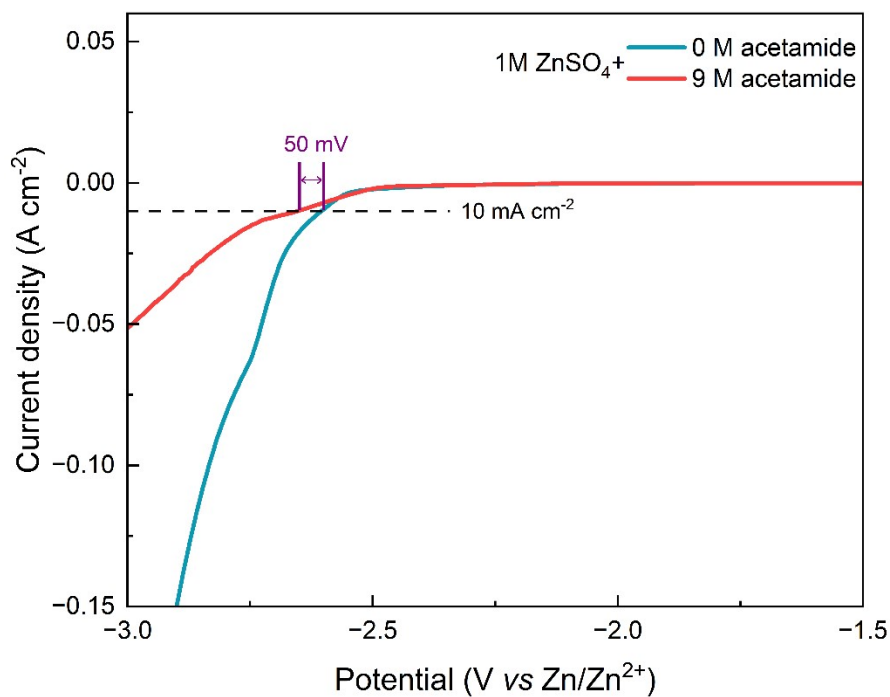
Fig. S10 Linear sweep voltammetry curves (LSV) tested in electrolytes with/without acetamide.

According to the theoretical calculation shown in Fig. 1f, acetamide molecules tend to form association structures with water molecules, and the original regular cross-linked structure between water molecules is destroyed. Thus, the activity of free water is limited, and HER is suppressed.[9, 10]
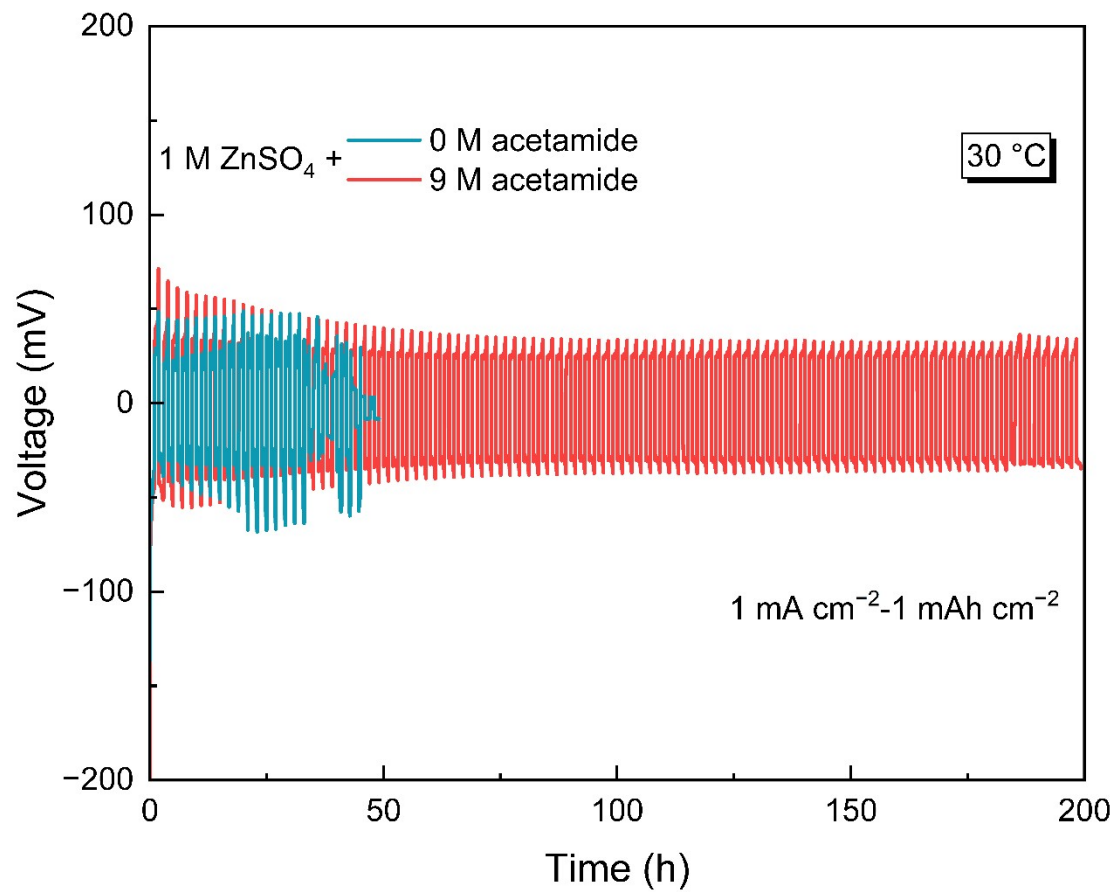
Fig. S11 Cycling performance of Zn||Zn cell using electrolytes with/without acetamide.
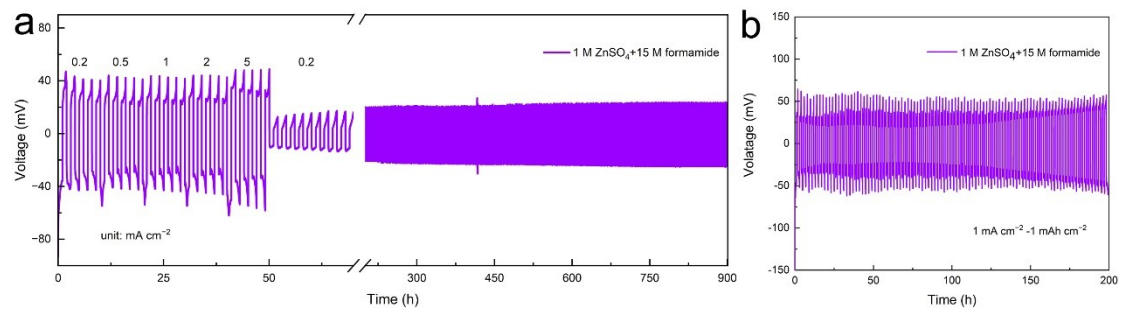
Fig. S12 Cycling performance of Zn||Zn cells using 1 M ZnSO$_4$ + 15 M formamide
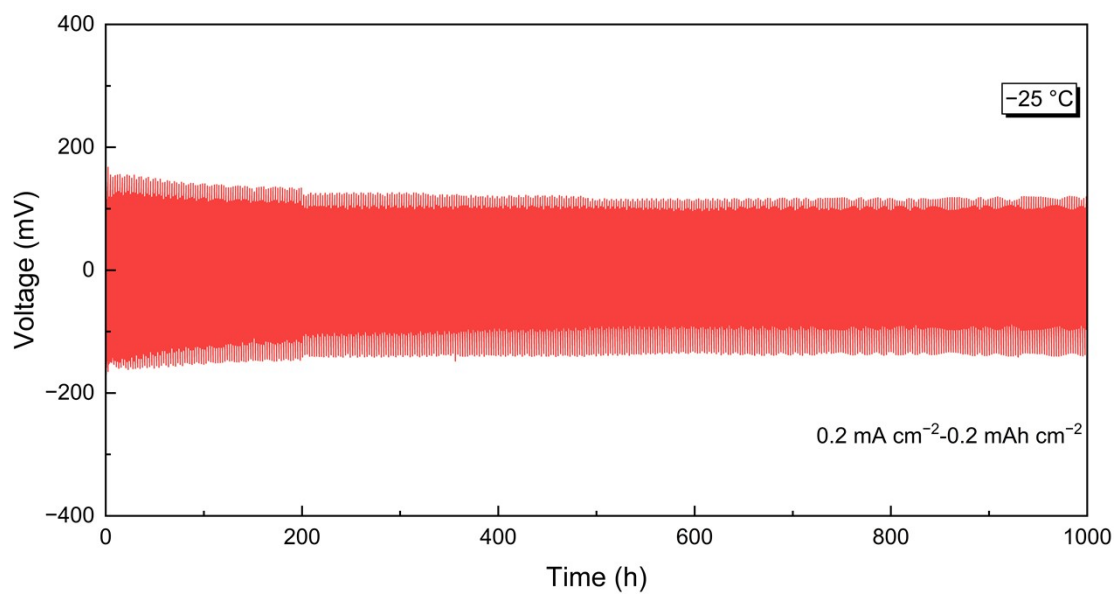
electrolyte at 30 °C.

Fig. S13 Cycling performance of Zn‖Zn cells using 1 M ZnSO$_4$ + 9 M acetamide electrolyte at −25 °C.
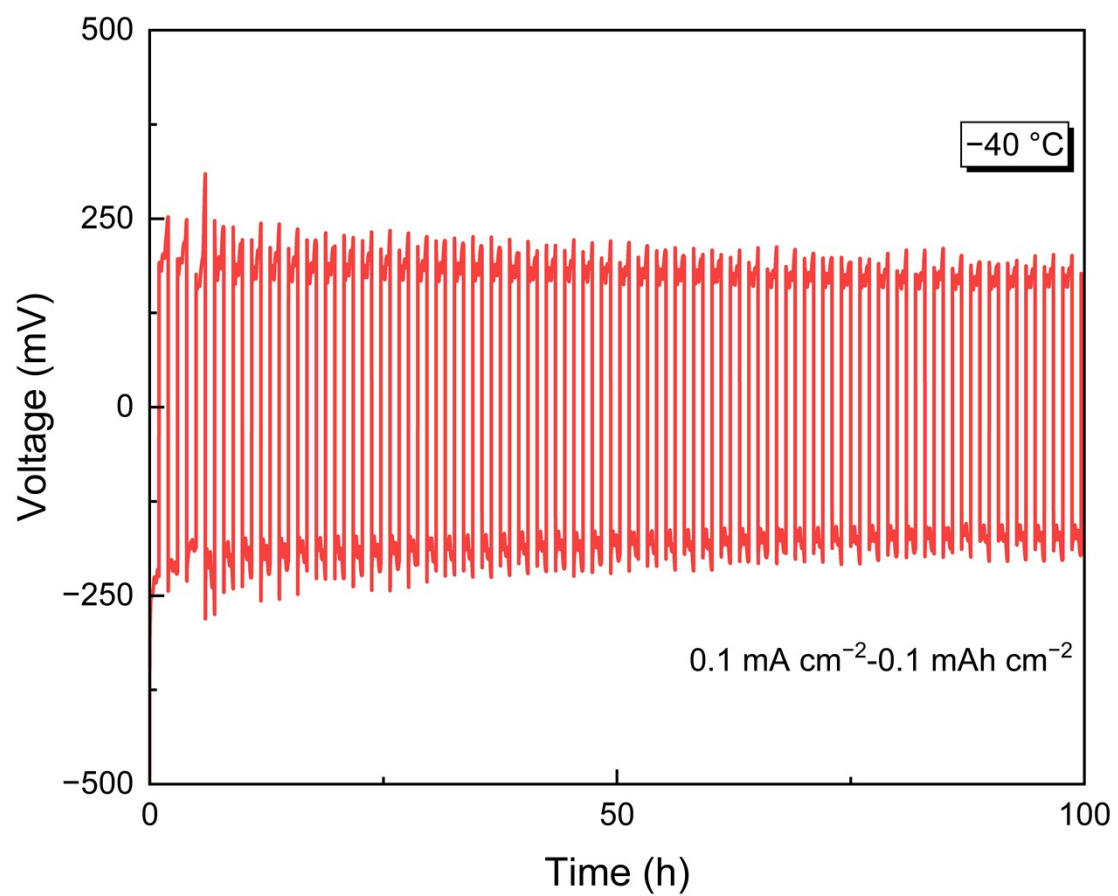
Fig. S14 Cycling performance of Zn‖Zn cells using 1 M $ZnSO_4$ + 9 M acetamide electrolyte at −40 °C.
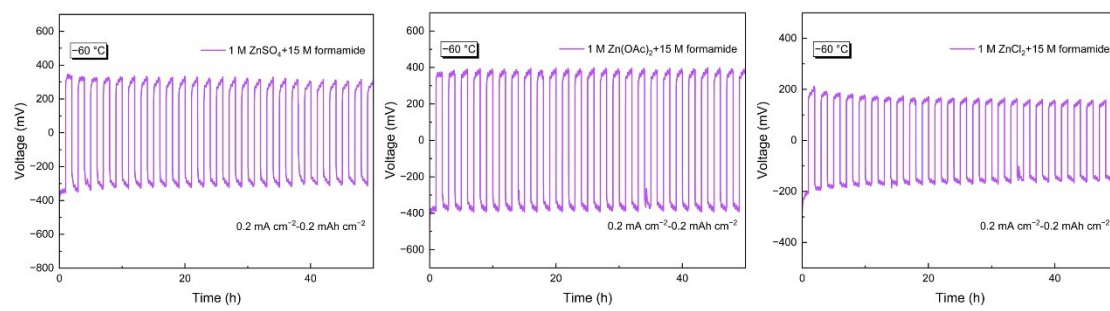
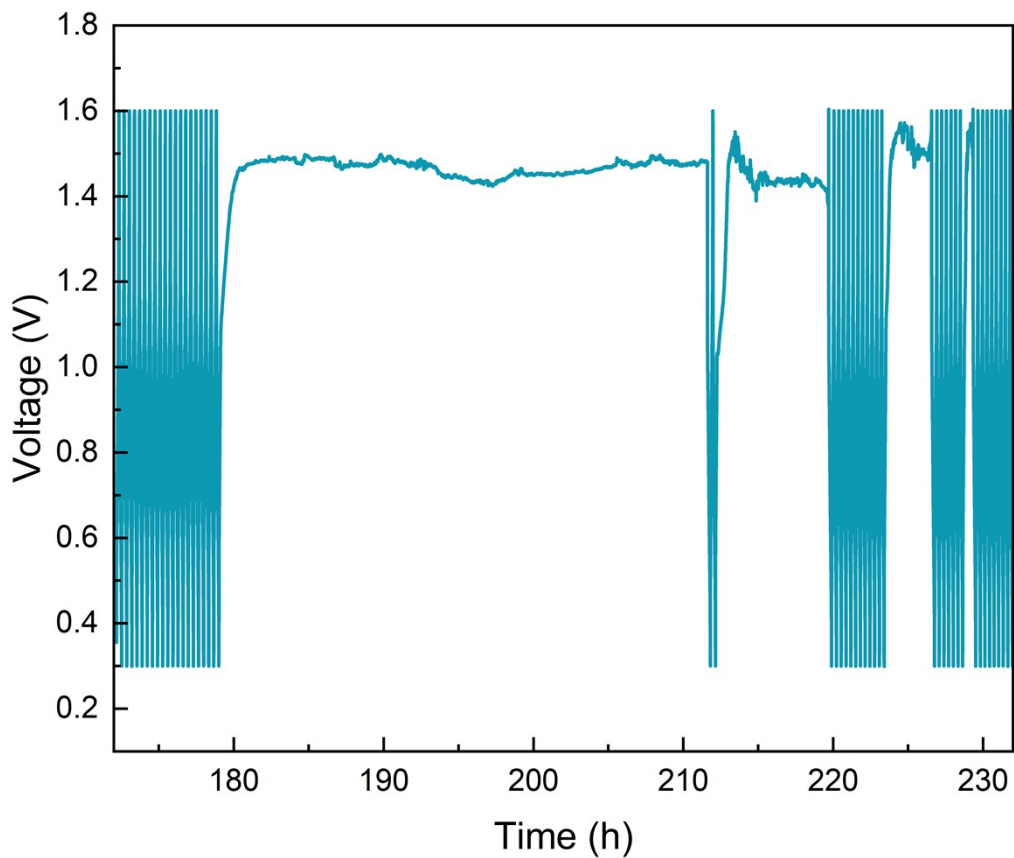Fig. S15 Cycling performance of Zn ‖ Zn cell using different electrolytes at −60 °C.

Fig. S16 The time-voltage curve of Zn‖PANI cell using electrolyte without acetamide addition.

The cell exhibited a severe overcharging phenomenon for more than 30 hours, probably caused by gas generation. In practical application scenarios, the battery is considered to have failed in the case of such an overcharging situation.
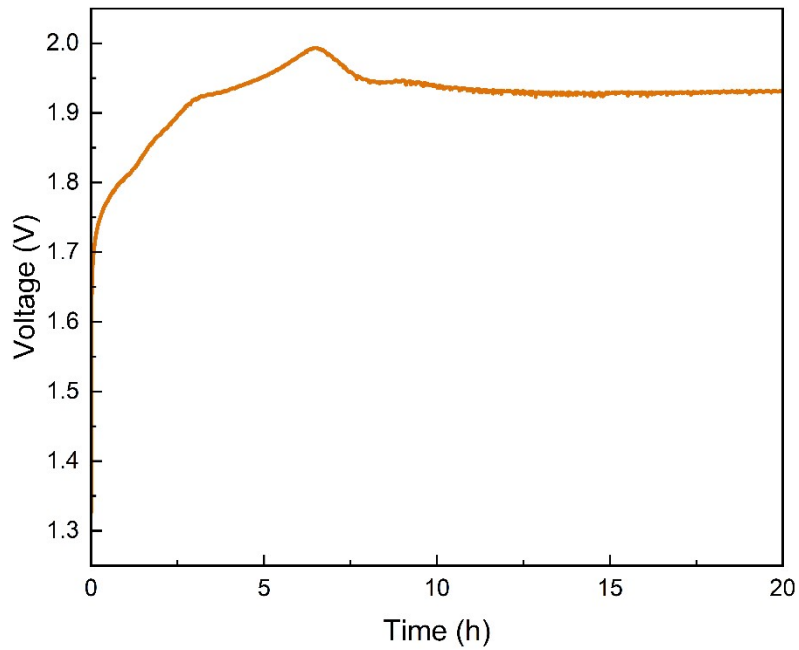
Fig. S17 The charge voltage profile of Zn||LMO full cell using 0.5 M ZnSO$_4$ + 0.5 M Li$_2$SO$_4$ electrolyte with a charging cut-off voltage of 2.05 V at a 0.1 C rate. The Zn||LMO cell suffers from voltage drop during charge process in 1 M ZnSO$_4$ normal electrolyte due to gas generation reactions of aqueous electrolytes.
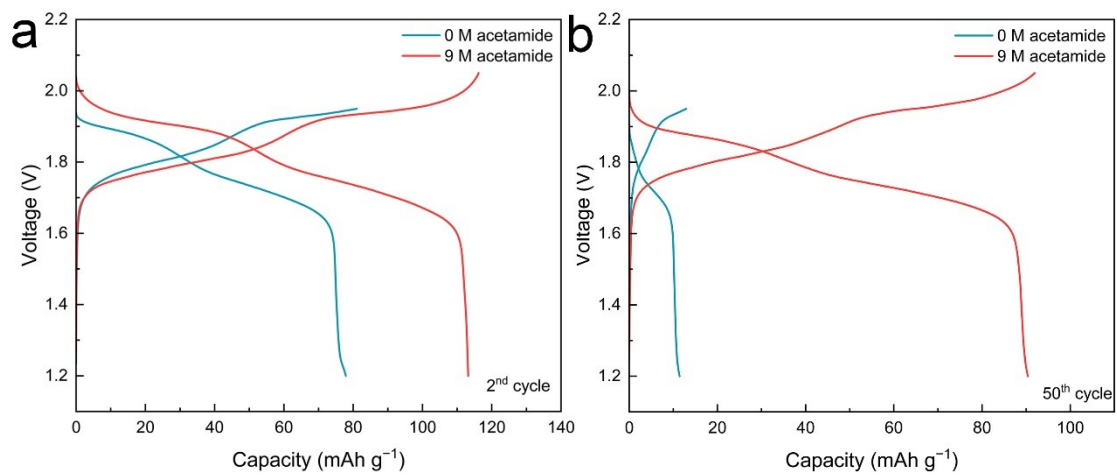
Fig. S18 The charge-discharge voltage-capacity curves of the Zn ‖ LMO full cell for (a) the 2nd and (b) 50th cycles.
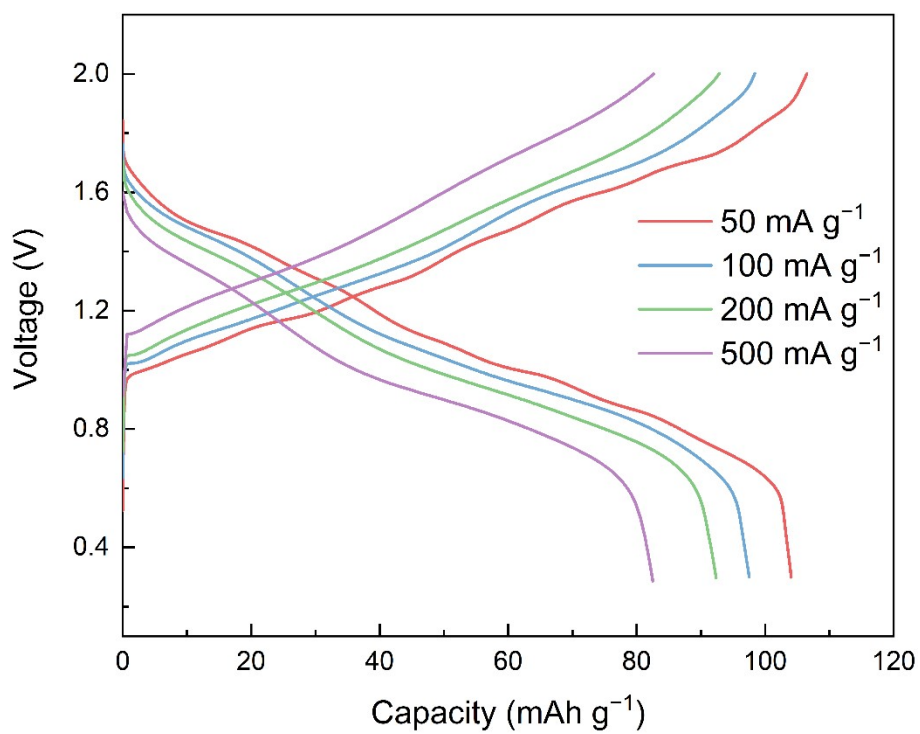
Fig. S19 The charge-discharge voltage-capacity curves of the Zn‖PANI full cell at −60
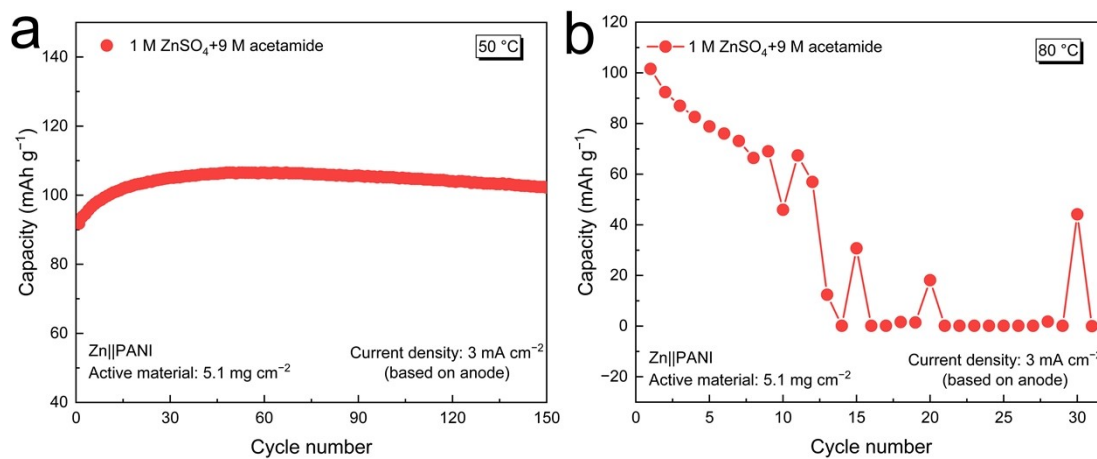
°C at different current densities.

Fig. S20 Cycling performance of Zn‖PANI cells using acetamide electrolyte at (a) 50 °C and (b) 80 °C.

The Zn‖PANI cell can still work stably at 50 °C with a high capacity. However, when the temperature increases to 80 °C, the cell can't work well and fails quickly.

References:

1. J. X. Huang and R. B. Kaner, *J. Am. Chem. Soc.*, 2004, **126**, 851-855.

2. L. Miao, R. Wang, S. Di, Z. Qian, L. Zhang, W. Xin, M. Liu, Z. Zhu, S. Chu, Y. Du and N. Zhang, *ACS Nano*, 2022, **16**, 9667-9678.

3. C. Lin, X. Yang, P. Xiong, H. Lin, L. He, Q. Yao, M. Wei, Q. Qian, Q. Chen and L. Zeng, *Adv. Sci.*, 2022, **9**, 2201433.

4. Y. Jin, K. S. Han, Y. Shao, M. L. Sushko, J. Xiao, H. Pan and J. Liu, *Adv. Funct. Mater.*, 2020, **30**, 2003932.

5. H. Wang, H. Du, R. Zhao, Z. Zhu, L. Qie, J. Fu and Y. Huang, *Adv. Funct. Mater.*, 2023, 2213803.

6. S. jiao, J. Fu, Q. Yin, H. Yao and H. Hu, *Energy Stor. Mater.*, 2023, **59**, 102774.

7. L. Cao, D. Li, E. Hu, J. Xu, T. Deng, L. Ma, Y. Wang, X.-Q. Yang and C. Wang, *J. Am. Chem. Soc.*, 2020, **142**, 21404-21409.

8. A. Rana, A. Thakare, N. Kumar, B. Mukherjee, A. Torris, B. Das, S. Ogale and A. Banerjee, *ACS Appl. Mater. Interfaces*, 2023, **15**, 23093-23103.

9. J. Xie, Z. Liang and Y.-C. Lu, *Nat. Mater.*, 2020, **19**, 1006-1011.

10. Y. Wang, T. Wang, D. Dong, J. Xie, Y. Guan, Y. Huang, J. Fan and Y.-C. Lu, *Matter*, 2022, **5**, 162-179.